ADVANCED FUNCTIONAL MATERIALS
www.afm-journal.de

Spiders Use Structural Conversion of Globular Amyloidogenic Domains to Make Strong Silk Fibers

*Xingmei Qi, Han Wang, Kezhen Wang, Yu Wang, Axel Leppert, Igor Iashchishyn, Xueying Zhong, Yizhong Zhou, Ruifang Liu, Anna Rising, Michael Landreh, Jan Johansson, and Gefei Chen**

Spider silk—an environmentally friendly protein-based material—is widely recognized for its extraordinary mechanical properties. Biomimetic spider silk-like fibers made from recombinant spider silk proteins (spidroins) currently falls short compared to natural silks in terms of mechanical performance. In this study, it is discovered that spiders use structural conversion of molecular enhancers—conserved globular 127-residue spacer domains—to make strong silk fibers. This domain lacks poly-Ala motifs but interestingly contains motifs that are similar to human amyloidogenic motifs, and that it self-assembles into amyloid-like fibrils through a non-nucleation-dependent pathway, likely to avoid the formation of cytotoxic intermediates. Incorporating this spacer domain into a recombinant chimeric spidroin facilitates self-assembly into silk-like fibers, increases fiber molecular homogeneity, and markedly enhances fiber mechanical strength. These findings highlight that spiders employ diverse strategies to produce silk with exceptional mechanical properties. The spacer domain offers a way to enhance the properties of recombinant spider silk-like fibers and other functional materials.

1. Introduction

Spider silk is a sustainable protein-based material renowned for its exceptional mechanical properties. The remarkable tensile strength surpasses that of numerous synthetic materials, making it a subject of scientific interest with vast potential in materials science, biotechnology, and medicine.[1] Spider silk is composed of spider silk proteins (spidroins), which are synthesized and secreted by specialized silk glands situated in the spider's abdomen.[1] These spidroins undergo a sophisticated process of assembly and spinning to form silk fibers.[2] At least seven distinct types of spidroins/glue exist, each possessing a unique sequence and properties. These include the major ampullate spidroin (MaSp), minor ampullate spidroin (MiSp), flagelliform spidroin (FlSp), aciniform spidroin (AcSp), tubuliform spidroin (TuSp),

X. Qi, H. Wang, R. Liu
The Jiangsu Key Laboratory of Infection and Immunity
Institutes of Biology and Medical Sciences
Soochow University
Suzhou 215123, China

K. Wang
School of Life Sciences
Anhui Medical University
Hefei, Anhui 230032, China

Y. Wang, A. Rising, J. Johansson, G. Chen
Department of Biosciences and Nutrition
Karolinska Institutet
Huddinge 14157, Sweden
E-mail: gefei.chen@ki.se

The ORCID identification number(s) for the author(s) of this article can be found under https://doi.org/10.1002/adfm.202315409

Y. Wang
College of Wildlife and Protected Area
Northeast Forestry University
Harbin 150040, China

A. Leppert, M. Landreh
Department of Microbiology, Tumor and Cell Biology
Karolinska Institutet
Solna 17165, Sweden

I. Iashchishyn
Department of Medical Biochemistry and Biophysics
Umeå University
Umeå 90187, Sweden

X. Zhong
School of Engineering Sciences in Chemistry, Biotechnology and Health
Department of Biomedical Engineering and Health Systems
KTH Royal Institute of Technology
Huddinge 14152, Sweden

Y. Zhou
Faculty of Food Science and Technology
Suzhou Polytechnic Institute of Agriculture
Suzhou 215008, China

DOI: 10.1002/adfm.202315409

pyriform spidroin (PySp), and aggregate silk glue (AgSg).[3,4] Each type of spidroin is used for spinning a specific type of silk or glue, endowed with precise biological functions and mechanical characteristics.[5] The MaSp, for instance, contributes to the production of dragline silk, known for its exceptional strength, while MiSp plays a role in creating the framework of capturing spirals in spider webs and does not super-contract in water.[6]

The challenging and impractical nature of harvesting silk from spiders necessitates an alternative approach. Consequently, focus has been on producing spidroins through recombinant DNA technology in various organisms such as bacteria, yeasts, animals, or plants.[5] These modified organisms can then generate substantial quantities of silk proteins, which can be harvested and processed into silk-like fibers or other materials.[7–10] Nonetheless, spidroins are large and repetitive proteins that pose challenges for recombinant protein expression. Therefore, expressing customized spidroins, that is, short repetitive regions capped by N- and C-terminal domains (NT and CT), followed by fiber preparation has become the prevalent strategy used for generating artificial spider silk-like fibers.[11–16] These designed chimeric spidroins with size range from 29 to 104 kDa can be spun into silk-like fibers by different approaches,[15,17–21] strongly suggesting that the production of chimeric spidroins, coupled with silk spinning, holds great potential for the creation of artificial spider silk. However, the resulting mechanical strength falls within a range of 50–245 MPa, which is considerably lower than that of natural spider silks.[5] The significance of high molecular weight in spidroins for achieving strong mechanical properties holds true not only for natural spider silks but also for recombinant spider silks, and this principle stands as a cornerstone in the pursuit of robust mechanical characteristics. Evidently, correlations have been established between the molecular weights of various customized spidroin variants and the ensuing mechanical attributes of the fabricated recombinant silk fibers.[22,23] These observations imply that augmenting the size of customized spidroins is able to serve as a viable approach to achieve the development of strong engineered silk fibers.

Various spidroins exhibit distinct compositions, characterized by divergent repetitive motifs or domains surrounded by relatively conserved globular NT and CT domains.[24] For instance, MaSp1 contains repetitive motifs such as GGX, GX, and poly-A, while MaSp2 is made up of GPX, QQ, GGX, GSG, and poly-A motifs.[25] In contrast, the MiSp sequence primarily comprises Gly and Ala residues organized into GX, GGX, GGGX motifs, and small amount of short poly-A motifs,[26] and FlSp is rich in GPGGX motifs.[27,28] In contrast, AcSp, TuSp, and PySp contain non-Gly-rich repetitive domains, ≈200 amino acid residues in length.[29–31] Notably, in MiSp and Flag, the repetitive Gly-rich motifs are interrupted by non-Gly-rich domains or stretches (**Figure 1a**), that have been designated as spacer region.[26] MiSp includes spacer domains spanning ≈127 amino acid residues, while FlSp contains multiple small spacer regions consisting of 9–27 amino acid residues that exhibit a higher propensity for β-sheet formation.[26,32] The functional significance of the larger spacer domains in MiSp has yet to be fully understood. Compared to MaSp, MiSp lacks poly-Ala motifs that are known for conferring silk mechanical strength[33] and is apparently smaller in molecular weight.[25,26] In spite of this, minor ampullate silk exhibits comparable strength to major ampullate silk.[5,6] This observation led us to hypothesize that the MiSp spacer domain might be a natural enhancer that can increase silk mechanical strength. To investigate this hypothesis, we here explore the phylogenetic origin, molecular properties, and functions of the MiSp spacer domain in spider silk formation.

2. Results and Discussion

2.1. AlphaFold Prediction of Spidroin Domains and Regions

To comprehensively delve into the phylogenetic and functional interconnections inherent in distinct regions of various spidroins/glue, this study focalizes on an in-depth investigation of the seven specific spidroin/glue proteins, that is, MaSp, MiSp, FlSp, AcSp, TuSp, PySp, and AgSg, originating from the common orb-weaving spider species *Araneus ventricosus*. In recent years, progress in genome sequence analysis has enabled the identification of numerous spidroins derived from various spider species. Furthermore, state-of-the-art technologies like Alphafold and RoseTTAfold have revolutionized protein structure predictions,[34,35] thereby providing the groundwork for protein sequence, structure, and function analysis. According to the predominant central repetitive region, the spidroins were grouped into two types, types I and II (Figure 1a), as previously reported.[36] In the type I group, the spidroins' central repetitive regions are built up by Gly, Ala, or Pro-rich motifs, for example, poly-A, GA, and GPGGX motifs, which are interrupted by spacers in Flag and MiSp (Figure 1a). Differently, in the case of type II spidroins, the repetitive subunits are ≈200 aa in size and are not dominated by the Gly, Ala, or Pro-rich motifs (Figure 1a). Based on predictions made by AlphaFold, the NT domains of the various spidroins exhibited a highly conserved tertiary structure (Figure 1b). This structure is characterized by a five-helix arrangement, which has been previously determined for recombinant *A. ventricosus* MiSp NT domain using nuclear magnetic resonance (NMR) spectroscopy.[37] A similar pattern was observed for the different CT domains, although the number of helices varied slightly among different spidroin types. For example, in FlSp, the CT domain consists of four helices as determined by NMR,[38] while MaSp2 CT exhibited six helices, and the remaining CT domains folded into five helices as predicted by AlphaFold (Figure 1c). These findings suggest that the evolutionary conservation extends beyond the amino acid sequences to the tertiary structures of both the NT and CT domains. This remarkable preservation in the terminal domains remains consistent across a diverse range of spidroins or glue, shedding light on the intricate mechanisms that govern the biological functions of these domains and highlighting their critical roles throughout evolutionary history.

A. Rising
Department of Animal Biosciences, Swedish University of Agricultural Sciences
Uppsala 75007, Sweden
G. Chen
Department of Cell and Molecular Biology
Uppsala University
Uppsala 75105, Sweden

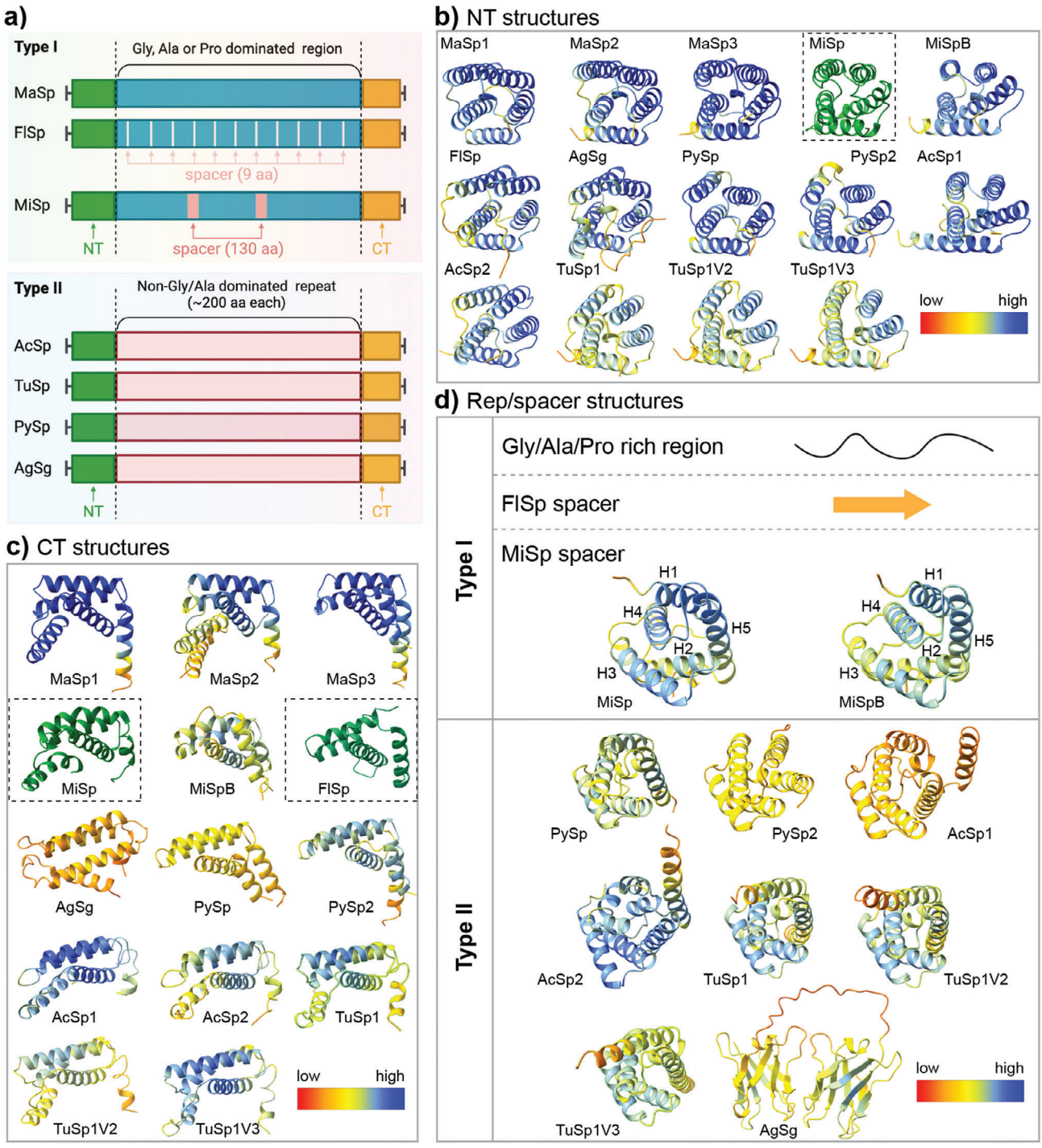

Figure 1. Structure predictions of different spidroin domains from *A. ventricosus* by AlphaFold. a) Architectures of different spidroins and glue from *A. ventricosus*. b) AlphaFold structure predictions of the NT domains of the different spidroins and glue. The color bar shows AlphaFold Coloring Dialog based on pLDDT confidence. The dashed box indicates the determined NMR structure. The accession number of the NT domains are MaSp1_NT (A0A4Y2GM25, position 24–150), MaSp2_NT (A0A4Y2KG20, position 25–153), MaSp3_NT (A0A4Y2MH26, position 26–151), MiSp_NT (pdb 2MX8), MiSpB_NT (A0A4Y2K2Y0, position 26–149), Flsp_NT (from ref.[17]), AgSg_NT (A0A4Y2BXZ1, position 35–162), PySp_NT (A0A4Y2SMB9, position 23–143), PySp2_NT (A0A6H1RJ79, position 23–141), AcSp1_NT (A0A6M3YBY8, position 29–163), AcSp2_NT (A0A7G7XXM9, position 28–160), TuSp1_NT (A0A221ZTM5, position 27–153), TuSp1V2_NT (A0A7D3QM03, position 27–153), TuSp1V3_NT (A0A7D3QKL5, position 27–153). c) AlphaFold structure predictions of the CT domains of the different spidroins and glue. The color bar shows AlphaFold Coloring Dialog based on pLDDT confidence. The dash boxes indicate NMR-determined structures. The accession number of the CT domains are MaSp1_CT (A0A4Y2GM25, position 2643–2757), MaSp2_CT (A0A4Y2KG20, position 2733–2870), MaSp3_CT (A0A4Y2MH26, position 2515–2618), MiSp_CT (pdb 2MFZ), MiSpB_CT (A0A4Y2K2Y0, position 2382–2484), Flag_CT (pdb 7VU7), AgSg_CT (A0A4Y2BY01, position 1537–1646), PySp_CT (A0A4Y2SMB9, position 3381–3520), PySp2_CT (A0A6H1RJ79,

In contrast to the non-repetitive terminal domains, the repetitive regions of the various spidroins displayed distinct structures. In the case of type I spidroins, namely MaSp, MiSp, and FlSp, the Gly, Ala, and Pro-rich motifs were predicted by AlphaFold to lack a specific folded structure, appearing as unstructured conformation (Figure 1d). However, it is worth noting that in Flag silk the small spacer region (9 aa) was predicted to adopt a β-strand structure, as previously reported.[26] Interestingly, the MiSp spacer was predicted to adopt a structure composed of five α-helices (Figure 1d), and this structure is conserved in MiSp spacer domains across different spider species[39] (Figure S1a, Supporting Information). In the type II spidroin group, despite very low sequence similarities between the subunits of PySp, AcSp, and TuSp (Figures S1d and S2, Supporting Information), their tertiary structures are surprisingly conserved (Figure 1d, **Figure 2a**). The subunits of PySp, AcSp, and TuSp all folded into α-helix structures, albeit with varying numbers of helices, in particular in the AcSp subunit (Figure 1d and Figure 2a). Furthermore, the structures of AcSp and TuSp (Figure S1b,c, Supporting Information) predicted by AlphaFold showed significant identities with the relevant NMR structures.[40,41] Interestingly, the repeat of AgSg differed in structure significantly from PySp, AcSp, and TuSp, as it was predicted with decent validity to adopt a two-layer β-sheet structure (Figure 1d). This unique structure of AgSg likely reflects its distinct biological function as glue rather than silk, as the formation of a dense, hydrogen-bonded β-sheet network is a structural attribute that likely contributes to the adhesive qualities of protein-based glues.[42]

A recent study discussed that the MiSp spacer found in the spider species *Nephila antipodiana* shares a similar structure with the AcSp and TuSp repetitive regions of the same spider species.[39] This structural similarity was also observed in the MiSp spacer of *A. ventricosus*, as its structure could be superimposed with the structures of AcSp and TuSp subunits (Figure 2b). Interestingly, the MiSp spacer also exhibited significant structure similarity to the PySp subunit (Figure 2b). Silk-like fibers can be drawn from as few as two repetitive regions from AcSp, $W_{AcSp}2$ (20–200 µmol L^{-1}) at pH 7.5,[43] which suggests that the MiSp spacer, TuSp and PySp subunits rather than the AgSg subunit might have the capability to assemble into fibers. And indeed, recombinant *N. antipodiana* MiSp spacer was reported to assemble into fibers induced by shearing force.[39]

The MiSp spacer domain was found to share a close phylogenetic relationship with PySp, AcSp, and TuSp, whereas the MiSp repetitive region (the Gly and Ala-rich region that contains typical MiSp repetitive motifs) was grouped with MaSp and Flag (Figure 2b). These findings suggest that the MiSp spacer and the Gly and Ala-rich region may have evolved independently. Furthermore, the grouping of MiSp with MaSp based on the NT and CT domains (Figure 2c), together with the clustering observed based on the Gly and Ala-rich regions (Figure 2b), indicates an evolutionary connection between MiSp and MaSp. It is likely that the spacer region in MiSp originated from type II spidroins through gene recombination,[44] but this hypothesis needs to be further investigated. These observations highlight the existence of two distinct evolutionary pathways for the repetitive regions of silk-forming spidroins: one characterized by sequences with low complexity and the other characterized by helical structures.

2.2. *A. ventricosus* MiSp Spacer Domain is Amyloidogenic

While the MiSp spacer domain is a specific evolutionary addition, the biological functions of the occurrence of type II-based spacer domain in type I MiSp remain unknown. Hence, the *A. ventricosus* MiSp spacer domain (amino acid sequence in Table S1, Supporting Information) was produced recombinantly with fused to a thioredoxin (Trx) tag in *Escherichia coli* and subsequently purified using immobilized metal affinity chromatography (IMAC), reverse-IMAC (after thrombin cleavage), and size exclusion chromatography (SEC). This purification process yielded tag-free proteins with a high degree of purity, as depicted in **Figure 3a**. The resulting recombinant spacer domain was monomeric, as evidenced by SEC analysis (Figure 3a), and folded into a predominantly α-helical structure, indicated by circular dichroism (CD) measurements (Figure 3b), supporting the prediction made by AlphaFold (Figure 1d). The recombinant spacer protein displayed a melting temperature of ≈50 °C (Figure 3c). Upon exposure to higher temperatures, it underwent denaturation, transitioning into a random coil conformation (Figure S3a, Supporting Information). This behavior is akin to the recombinant MiSp NT domain, but not the recombinant CT domain that unfolds and refolds into β-sheets with increasing temperature.[2,37] In a recent investigation, it was observed that the recombinant *N. antipodiana* MiSp spacer (with a His_6-tag) exhibited pH sensitivity and greater stability at higher pH levels.[39] However, the recombinant *A. ventricosus* MiSp spacer did not display significant pH sensitivity. CD analysis revealed no noticeable changes in secondary structure and thermo-stability across pH levels ranging from 7.5 to 5.5 (Figure 3b,c). Additionally, at pH 8.0, the recombinant spacer proteins adopted a monomeric conformation (Figure 2a) and remained stable when the pH was reduced from 8.0 to 5.5, as confirmed by electrospray ionization mass spectrometry (ESI-MS, Figure 3d).

position 2016–2155), AcSp1_CT (A0A6M3YBY8, position 3638–3746), AcSp2_CT (A0A7G7XXM9, position 4634–4745), TuSp1_CT (A0A221ZTM5, position 1811–1921), TuSp1V2_CT (A0A7D3QM03, position 4626–4736), TuSp1V3_CT (A0A7D3QKL5, position 4272–4382). d) AlphaFold structure predictions of the repetitive and spacer regions of the different spidroins and glue. The color bar shows AlphaFold Coloring Dialog based on pLDDT confidence. The yellow schematic arrow represents β-strand. The accession number of the amino acid sequences of the repetitive regions are MaSp1_rep (A0A4Y2GM25, position 359–558), MaSp2_rep (A0A4Y2KG20, position 196–395), MaSp3_rep (A0A4Y2MH26, position 378–577), MiSp_rep (K4MTL7, position 297–496), MiSpB_rep (A0A4Y2K2Y0, position 1523–1722), PySp_rep (A0A4Y2SMB9, position 377–589), PySp2_rep (A0A6H1RJ79, position 1386–1611), AcSp1_rep (A0A6M3YBY8, position 579–766), AcSp2_rep (A0A7G7XXM9, position 384–566), TuSp1_rep (A0A221ZTM5, position 530–727), TuSp1V2_rep (A0A7D3QM03, position 1241–1438), TuSp1V3_rep (A0A7D3QKL5, position 1239–1436), AgSg_rep (A0A4Y2BXZ1, position 1733–1940). The accession number of the amino acid sequences of the spacer regions are Flag_spacer (A0A4Y2M3Y8, position 1205–1213), MiSp_spacer (K4MTL7, position 991–1117), MiSpB_spacer (A0A4Y2K2Y0, position 1723–1849). [Correction added on April 19, 2024, after first online publication: a typo in figure 1a was corrected in this version.]

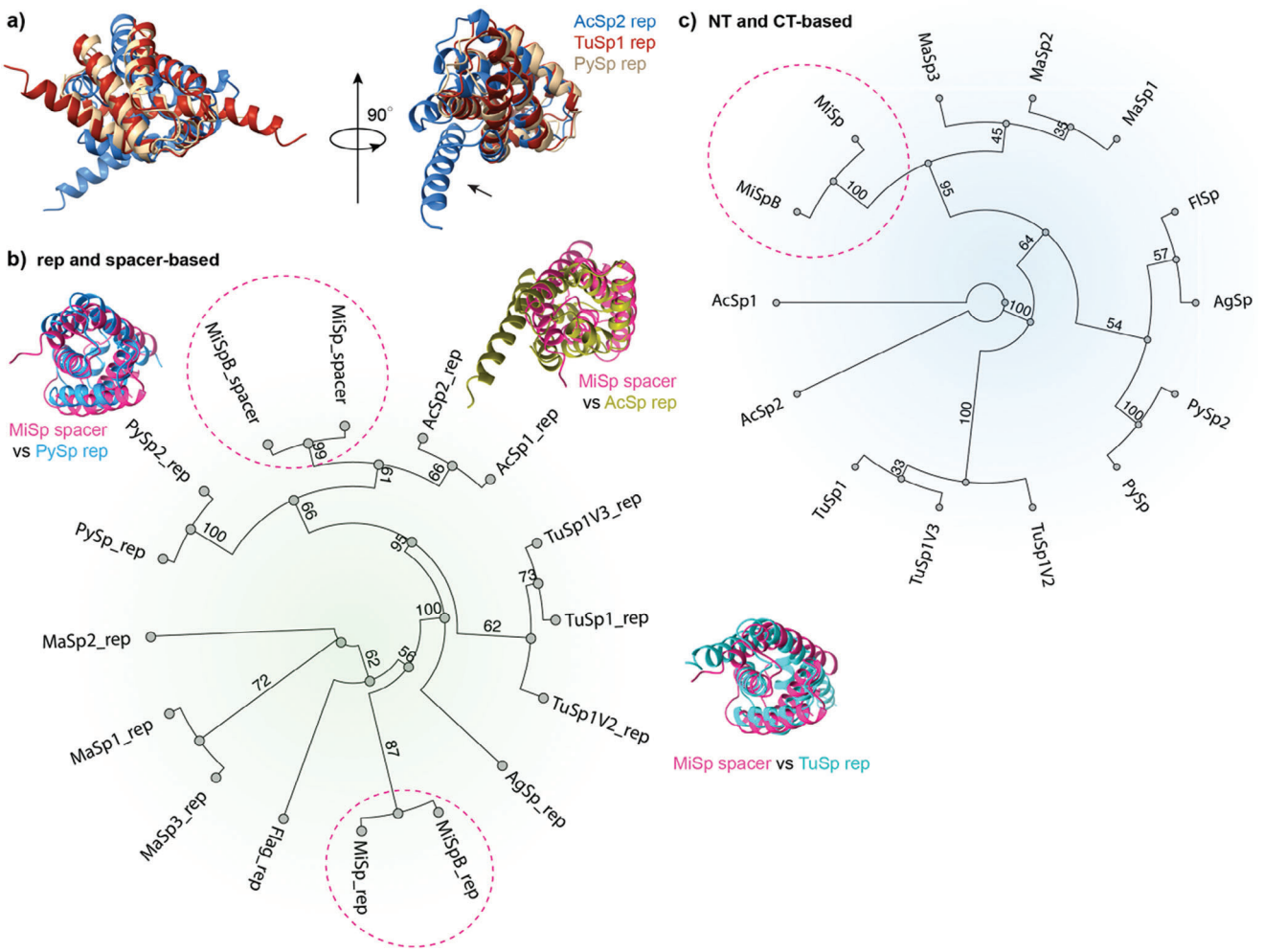

Figure 2. Evolutionary grouping of different spidroins based on *A. ventricosus* terminal domains, repetitive and spacer regions. a) Structure comparison of subunits from the repetitive regions of PySp, AcSp2, and TuSp1. The arrow indicates the extra helix in AcSp subunit. b) Phylogenetic analysis of the *A. ventricosus* spidroins based on the sequences from the repetitive (rep) and spacer regions. The dashed circles highlight MiSp. Structure comparisons of MiSp_spacer versus PySp_rep, MiSp_spacer versus AcSp_rep, and MiSp_spacer versus TuSp_rep are shown along the evolutionary groups. (c) Phylogenetic analysis of the different *A. ventricosus* spidroins based on the combinations of terminal domains. The dashed circle highlights MiSp. The branch values indicate the bootstrap values.

An intriguing observation was made with the recombinant *A. ventricosus* MiSp spacer proteins during overnight incubation under quiescent conditions. Instead of remaining in a monomeric state, the proteins formed large aggregates. Native mass spectrometry confirmed the complete loss of soluble species, showing instead a raised baseline associated with the presence of aggregates (Figure 3d). The aggregates displayed positive staining with the amyloid-specific dye thioflavin T (ThT), suggesting the presence of amyloid-like fibrils. Furthermore, the secondary structure underwent a transition from α-helix to β-sheet conformation during the transformation from monomers to aggregates (Figure 3g). Transmission electron microscopy (TEM) revealed the presence of amyloid-like fibrils with an approximate diameter of 10 nm (Figure 3h). This indicates that recombinant *A. ventricosus* MiSp spacer has the capacity to self-assemble into amyloid-like fibrils in physiological buffer within a broad pH range under quiescent conditions.

Amyloid formation is often a nucleation-elongation-dependent process, where fibril growth requires the formation of an oligomeric nucleus. Furthermore, fibril formation can be facilitated by the addition of preformed aggregates, known as seeding effects.[45] Typical examples for this aggregation mechanism are pathogenic Alzheimer's disease (AD) associated amyloid-β (Aβ) peptide,[46] which can also form silk-like fibers by hand-pulling strategy if placed between NT and CT domains.[36] Amyloidogenic polymerization from monomers can also occur via a non-nucleation-dependent polymerization pathway, where the association constants for monomer addition to any protein species are identical.[45] This mechanism has been recently found for the CT domain and repetitive regions of recombinant *A. ventricosus* MiSp and AcSp.[36] To dissect the amyloid fibril formation mechanism, we performed a series of ThT measurements on the recombinant MiSp spacer at 37 °C under quiescent conditions with different initial monomer concentrations (Figure 3e). The final fluorescence intensity exhibited a linear dependence on the

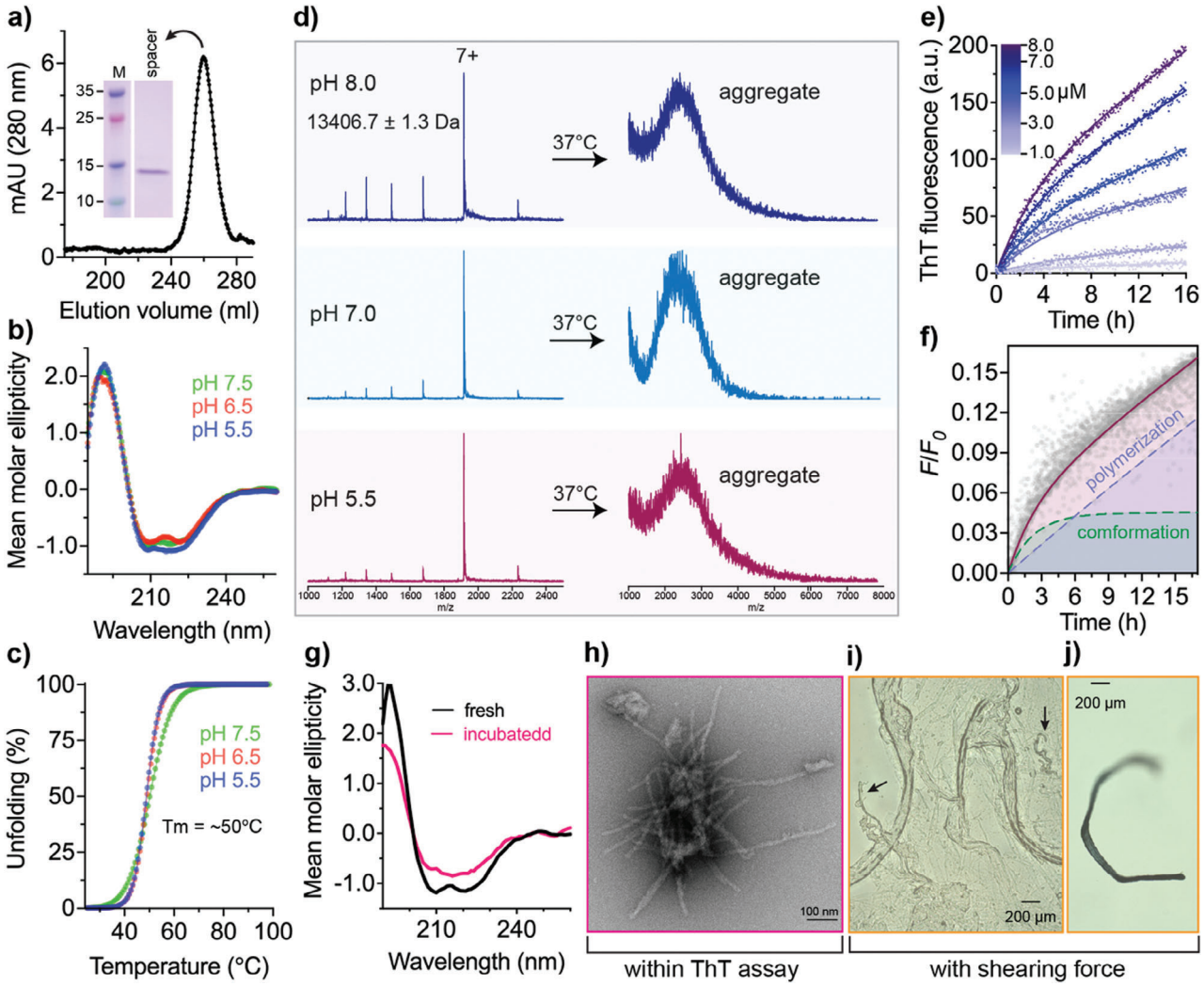

Figure 3. Characterization of the recombinant *A. ventricosus* MiSp spacer domain. a) Gel filtration and SDS-PAGE analysis of the recombinant MiSp spacer. b) CD spectra of the recombinant spacer at pH 7.5, 6.5, and 5.5. The Y-axis is the mean molar ellipticity in deg·cm^2·dmol^{-1} (× 10^4). c) Temperature-induced unfolding of the recombinant MiSp spacer. The CD signal was measured at 222 nm at pH 7.5, 6.5, and 5.5 and converted to mean residue ellipticity in deg·cm^2·dmol^{-1}. d) ESI-MS spectra of the recombinant MiSp spacer before and after overnight incubation at 37 °C at pH 8.0, 7.0, and 5.5. The charge states and the molecular weight are indicated in the pH 8.0 spectrum. e) Aggregation kinetics of recombinant MiSp spacer at 1.0, 2.0, 4.0, 5.0, 7.0, and 8.0 µmol L^{-1} in 20 mmol L^{-1} NaPi pH 8.0 at 37 °C under quiescent conditions. The traces were globally fitted with a two-phase exponential equation. f) The normalized fluorescence kinetics (from panel e) of the recombinant spacer domain. The polymerization term is indicated by a light blue dashed line, the conformation term by a green dotted line, and their sum by a solid dark red line. g) CD spectra of the recombinant spacer before and after incubation at 37 °C at pH 8.0. h) Transmission electron microscopy image of incubated recombinant MiSp spacer at pH 8.0. The scale bar is 100 nm. i,j) Light microscopy images of incubated recombinant MiSp spacer at pH 8.0 with shearing force. The scale bars are 200 µm. The arrows indicate silk-like fibers.

initial monomer concentration (Figure S3b, Supporting Information), suggesting that ThT reports accurately on the reaction progress, as previously reported for other spidroin amyloidogenic peptides.[36] For all the tested concentrations of the recombinant MiSp spacer domain, the shape of kinetic traces was hyperbolic, that is, no lag phase, indicating that neither monomer-dependent secondary nucleation[47] nor oligomer-dependent polymerization seems to be the rate-limiting step.[45] Furthermore, after data normalization, the aggregation traces for different spacer concentrations overlapped (Figure S3c, Supporting Information), which indicates that the aggregation constants at different concentrations are identical, suggesting a non-nucleation-dependent aggregation mechanism, similar to the recombinant MiSp and AcSp repetitive regions and the CT domain.[36] Furthermore, the aggregation traces of different recombinant spacer concentrations were fitted globally (Figure 3e), and could be described well with the two terms model—polymerization and conformational change (Figure 3f), where k_r was 1.9×10^{-11} M^{-1} s^{-1} and k_c was 1.1×10^{-9} M^{-1} s^{-1}.

In addition to the formation of amyloid-like fibrils, the recombinant *A. ventricosus* MiSp spacer was able to assemble into films and macroscopic silk-like fibers when subjected

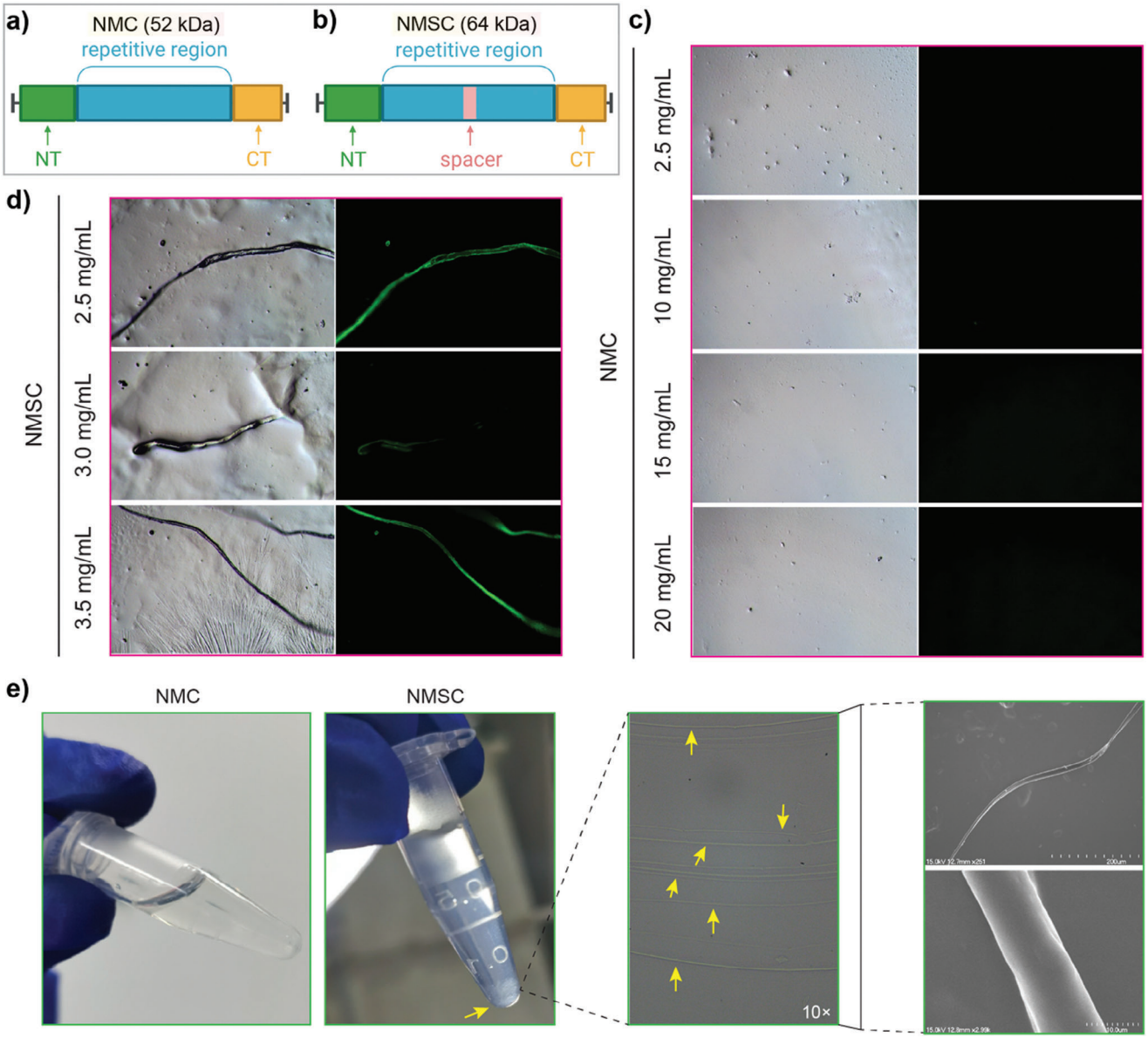

Figure 4. Self-assembly of the chimeric spidroin NMC and NMSC. a,b) Schematic architectures of the chimeric spidroin NMC and NMSC. c,d) Self-assembly of NMC and NMSC at different concentrations under pH 7.5. The silk-like fibers were imaged by a fluorescent microscope. e) Self-assembly of recombinant NMC and NMSC within an Eppendorf tube at pH 7.0 (at pH 6.0 and 5.0 see Figure S4c, Supporting Information). The yellow arrows indicate silk-like fibers. The silk-like fibers were imaged by inverted fluorescence and scanning microscopy. The scale bars are 200 µm (top) and 10 µm (bottom).

to shearing force (Figure 3i,j). This suggests that the spacer protein can self-assemble into amyloid-like nanofibrils, films, and silk-like fibers depending on the experimental conditions.

2.3. MiSp Spacer Domain Facilitates Silk-Like Fiber Formation

To investigate the molecular functions of the MiSp spacer domain in spider silk formation, two chimeric proteins were generated based on the complete *A. ventricosus* MiSp amino acid sequence.[26] These chimeric proteins were named NT_{MiSp}-M_{MiSp}-CT_{MiSp} (NMC) and NT_{MiSp}-M_{MiSp}-S_{MiSp}-CT_{MiSp} (NMSC), where "M" represents the Gly/Ala-rich region of MiSp and "S" represents the spacer domain (**Figure** 4a,b, amino acid sequences in Table S1, Supporting Information). Both NMC and NMSC proteins were expressed in *E. coli* and purified (Figure S4a, Supporting Information). Judged by CD measurements, both recombinant proteins, NMC and NMSC, primarily adopted an α-helical structure, which can be attributed to the α-helical nature of the NT and CT domains[2,37] as well as the spacer domain (Figure 3b). The NMC protein displayed a relatively higher proportion of random coil regions compared to the NMSC protein, which is likely due to the relatively higher percentage of the unstructured

repetitive regions (M) within the NMC sequence (Figure S4b, Supporting Information).

To evaluate the influence of the spacer domain on the self-assembly of MiSp into silk fibers, we conducted experiments where recombinant NMC or NMSC proteins at different concentrations in a 10 mmol L^{-1} Tris pH 7.5 solution were subjected to fiber-pulling using a tip (Figure 4c,d). Remarkably, regardless of the initial tested protein concentrations, silk-like fibers were successfully generated from the recombinant NMSC proteins (Figure 4d). In contrast, no fibers were formed from recombinant NMC proteins, even at initial concentrations up to 20 mg mL^{-1} (Figure 4c). These observations indicate that the MiSp spacer domain plays a crucial role in facilitating the assembly of the chimeric spidroins into silk-like fibers. Furthermore, in an Eppendorf tube at pH 7.5, the recombinant NMSC proteins self-assembled into fibers with an approximate diameter of 10 μm at a concentration of 2.5 mg mL^{-1} (Figure 4e). In contrast, the recombinant NMC did not exhibit any signs of silk-like fiber formation (Figure 4e). As expected from the pH sensitivity of the terminal domains CT and NT,[2,37] the recombinant NMSC demonstrated pH-dependent fiber formation. Notably, at pH 5.0, a significantly higher number of silk-like fibers were formed by recombinant NMSC proteins, while NMC did not exhibit visible silk-like fiber formation at the tested protein concentrations and pH levels (Figure S4c,d, Supporting Information).

2.4. MiSp Spacer Domain Enhances the Mechanical Strength

To evaluate the impact of the MiSp spacer domain on the mechanical properties of silk fibers, we prepared solutions of lyophilized recombinant NMC or NMSC proteins in 100% hexafluoroisopropanol (HFIP) at various concentrations (100, 80, 50, and 30 mg mL^{-1}). These protein stocks were then incubated at 37 °C for several hours and subsequently centrifuged to remove any undissolved protein. The resulting supernatant, containing the recombinant NMC or NMSC proteins, was collected as the wet spinning stock (**Figure 5a**). We then spun the recombinant NMC and NMSC at different concentrations into a coagulation bath consisting of varying concentrations of methanol (Table S2, Supporting Information). When the protein concentration was low (30 mg mL^{-1}), we were able to spin silk-like fibers from the recombinant NMSC proteins using methanol concentrations of 90% and 100%. However, no fibers were generated for NMC, regardless of the methanol concentration used (Table S2, Supporting Information). At higher protein concentrations (80 and 100 mg mL^{-1}), both the recombinant NMC and NMSC proteins could be spun into silk-like fibers at different methanol concentrations. However, under most conditions, the NMC proteins tended to form fragile fibers that were difficult to collect (Table S2, Supporting Information). To compare the mechanical properties of the NMC and NMSC fibers, we selected a protein concentration of 80 mg mL^{-1} and a methanol concentration of 85%. Under these conditions, both NMSC and NMC proteins were able to generate silk-like fibers that could be collected and tested (Figure 5b).

The diameter of NMSC fibers (≈14 μm) was smaller than that of NMC (≈20 μm) (Figure 5c). This suggests that the presence of the MiSp spacer domain may promote a more compact alignment of the protein chains in the fibers. We then proceeded to measure the mechanical properties of the recombinant NMC and NMSC silk-like fibers (Figure 5d). Surprisingly, the NMSC fibers exhibited significantly higher strength and toughness compared to the NMC fibers (Figure 5e–i). Native minor ampullate silks from different spider species demonstrate varying levels of ultimate strength, while for *Argiope trifasciata* and *Nephila inaurata* these silks possess a range of ultimate strength between 920 and 1400 MPa.[5] The average strength of NMSC fibers could reach up to 352±123 MPa, ≈2.8 times higher than that of NMC fibers (124±89 MPa) (Figure 5e–g). However, the extensibility of NMC and NMSC fibers was similar (Figure 5h). These results indicate that the MiSp spacer domain can enhance the mechanical strength of the fibers without significantly affecting their extensibility. To investigate the underlying mechanism behind the differences in mechanical properties, the fibers were subjected to secondary structure analysis using Fourier-transform infrared spectroscopy (FTIR). Although there was a slight tendency for higher β-sheet content in NMSC fibers compared to NMC fibers (Figure 5j; Figure S5, Supporting Information), there were no significant differences regarding the secondary structure content between fibers spun from these two proteins. Thus, FTIR spectroscopy did not detect any notable variations in the secondary structure content of these different fibers, as reported for other recombinant silks.[48] To further investigate the potential difference between the two different silk-like fibers, we used confocal laser scanning microscopy to observe the internal fiber features. As shown in Figure 5k, the NMC fibers displayed many dark areas along the fiber axis. The fluorescence of NMSC fibers was more homogeneous, and obvious large dark areas were not observed. These results suggest that the MiSp spacer domain can improve the intrinsic molecular homogeneity of the relevant fibers.

In a recent correlation analysis employing accessible data on the mechanical properties of synthetic spider MaSp/MiSp silk fibers, findings suggested that an elevated count of poly-Ala repeats, and consequently, a higher molecular weight of the engineered spidroin is linked to enhanced fiber strength, specifically in post-stretched fibers,[49] suggesting the importance of high molecular weight in spidroins for achieving strong mechanical properties. Indeed, various approaches have been explored to generate larger recombinant spidroins, such as intein-mediated splicing,[50–52] transgenic silkworm techniques,[53] and engineered *E. coli*.[22] However, it is worth noting that natural spider silks also possess high strength despite apparently having relatively small spidroins. For instance, the MiSp (≈150 kDa[26]) is approximately two-fold smaller than MaSp (≈300 kDa[25]). Furthermore, compared to MaSp, MiSp lacks a significant number of poly-Ala motifs that contribute to silk mechanical strength.[33] Nonetheless, minor ampullate silk exhibits comparable strength to major ampullate silk,[5,6] highlighting the potential role of the specific MiSp spacer domain as an enhancer of mechanical strength in natural silks. In fact, despite its relatively small size (64 kDa), silk fibers derived from NMSC exhibited an average mechanical strength of ≈352 MPa (Figure 5e–g), similar to or better than most of the silk-like fibers derived from recombinant spidroins of a similar size.[49] This improvement in mechanical strength is attributed to the spacer domain by facilitating the formation of a more compact alignment of protein chains in the fibers, supported by the significantly smaller

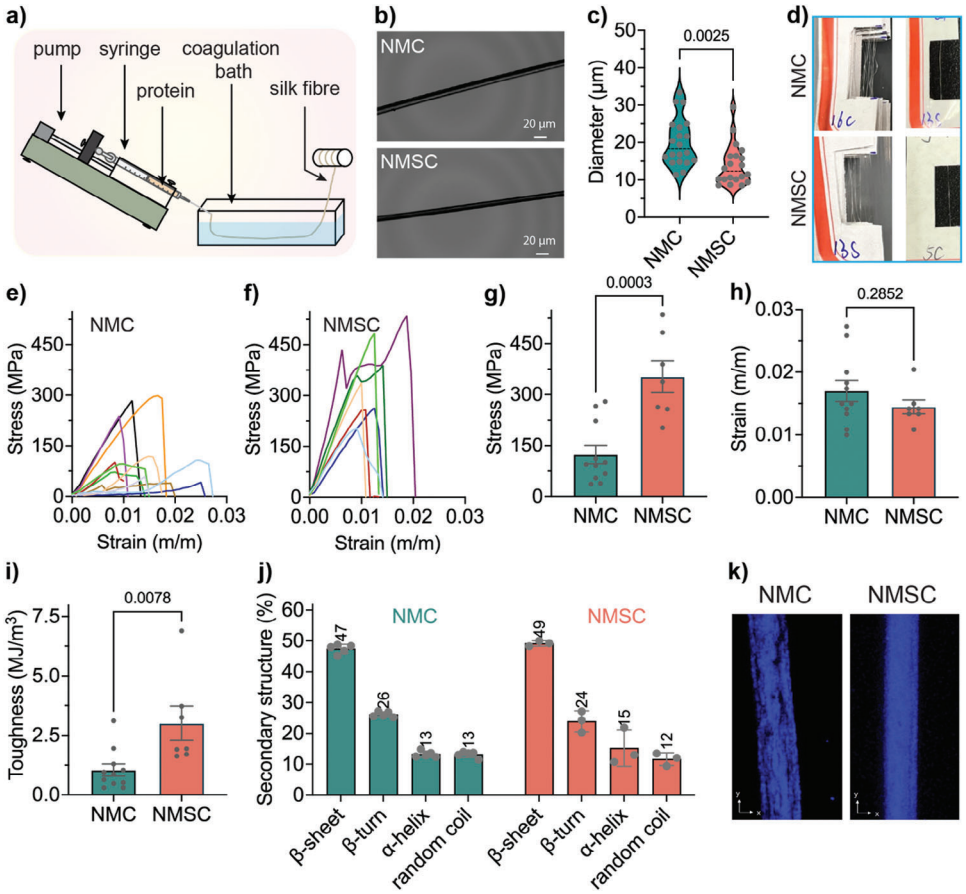

Figure 5. Recombinant silk fiber preparation and characterization. a) Schematic representation of the spinning device. The lyophilized protein powder of recombinant NMC or NMSC proteins were collected in a 29G syringe with a needle and pushed into the coagulation bath through a pump. The spinning rate was 10 μL min^{-1}, and the coagulation bath was 85% methanol (v/v). The silk collector was set up with a distance (≈12 cm) from the position where the silk-like fibers formed. b) Imaging of silk-like fibers derived from recombinant NMC and NMSC by confocal microscopy. The scale bars are 20 μm. c) The diameters of NMC and NMSC silk-like fibers. Data are presented as mean ± SD, and the statistical significance was assessed by unpair student's t-test. For each group, 20 fibers were measured. d) Representative NMC and NMSC silk-like fiber samples collected on paper frame for mechanical tests. e,f) Stress–strain curves showing individual tests for recombinant NMC and NMSC silk-like fibers generated by wet spinning. At least 10 samples for each fiber type were tested. g–i) Comparisons of mechanical stress, strain, and toughness of the silk-like fibers from recombinant NMC and NMSC proteins. Data are presented as mean ± SD, and the statistical significance was assessed by unpair student's *t*-test. j) Secondary structure content of NMC and NMSC fibers, determined by their absorbance spectra within the amide I region. k) Confocal laser scanning microscopy images of NMC and NMSC fibers, which were visualized based on their intrinsic fluorescence.

diameters of the fibers observed (Figure 5c) and the intrinsic fluorescence distribution (Figure 5k). It has been shown that larger proteins only give stronger fibers if the fibers are post-stretched, which is likely due to the forming of more aligned proteins during this procedure,[49] supporting the importance of molecular homogeneity with regard to fiber mechanical properties.

2.5. MiSp Spacer Domain Shares Common Motifs Found in Human Pathogenic Amyloidogenic Peptides

The detailed molecular mechanism on how the amyloidogenic MiSp spacer domain improves molecular homogeneity needs to be further investigated. Recently, hybrid polypeptides that combine spider silk glycine-rich segments with non-spider amyloid peptides have been generated. For instance, Li et al. have successfully wet-spun hybrid polypeptides that were dissolved in HFIP, comprised of alternating spider silk glycine-rich segments from *Nephila clavipes* MaSp1 and short human pathogenic amyloid peptide motifs, such as GDVIEV from αB-crystallin, KLVFFAE from A*β*, and FGAILSS from islet amyloid polypeptide (IAPP), into macroscopic fibers with exceptional tensile strength.[54] Moreover, promising results have been observed by modifying the amino acid sequence of the poly-Ala motif in MaSp1, which enhances its amyloidogenic propensity and leads to improved mechanical properties of biomimetic spider silk fibers.[48] These advancements underscore the potential of hybrid polypeptides that combine short amyloidogenic fragments and spider silk segments in the development of high-strength fibers.

Close analysis of the amino acid sequence revealed that the MiSp spacer domain, interestingly, contains regions that are similar to amyloid-forming motifs in human pathogenic peptides A*β*42 and IAPP (**Figure 6a**). Moreover, these motifs, SQNVIN (motif I) and SNAGAIN (motif II) were predicted to be capable

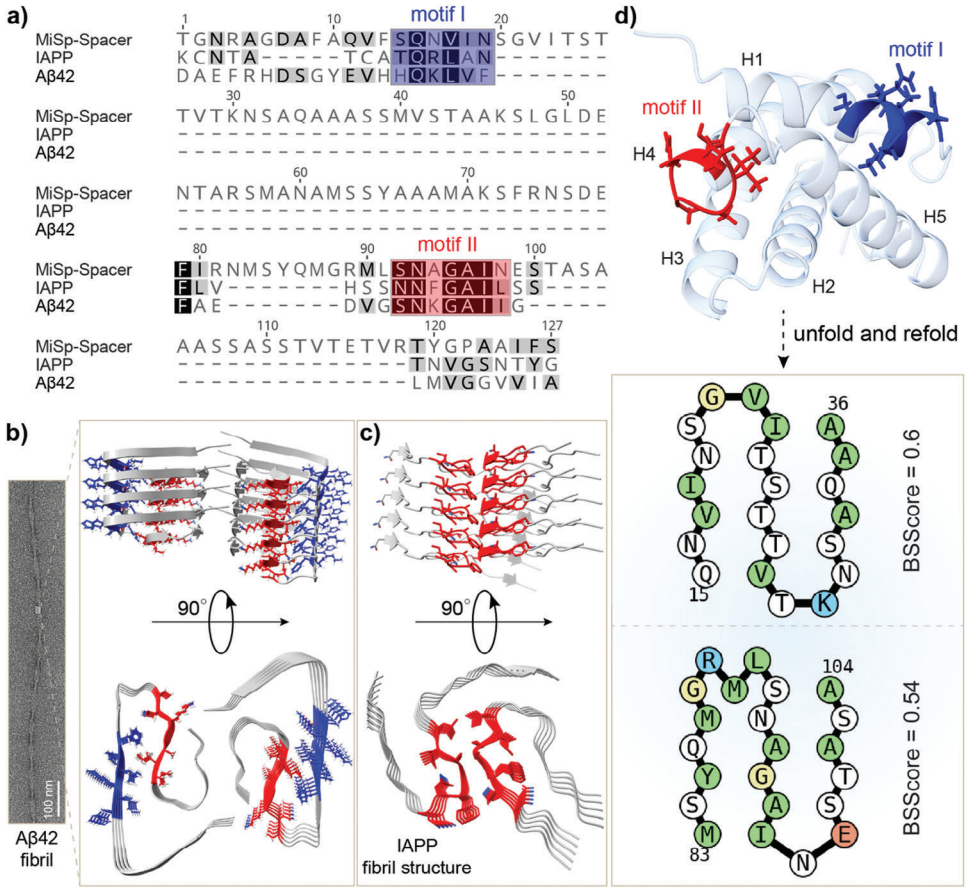

Figure 6. Amyloid-forming motifs in *A. ventricosus* MiSp spacer domain. a) Amino acid sequence comparison of *A. ventricosus* MiSp spacer domain, human Aβ42 and IAPP peptides. The motifs I and II are shadowed in blue and red, respectively. b,c) CryoEM structures of Aβ42 and IAPP fibrils (pdb: 5OQV and 7M61). Motifs I and II are shown in stick in blue and red, respectively. d) AlphaFold structure of *A. ventricosus* MiSp spacer domain. The helices are labeled with H1–5, and the motifs I and II are shown in blue and red. The β-serpentine arrangements of *A. ventricosus* MiSp spacer amyloid-like structure were predicted by BetaSerpentine,[58] and the representative β-serpentines, featuring motifs I and II, are shown. The BSScore, a comprehensive composite score, is derived from four distinct measures: MAScore, CompactScore1, CompactScore2, and TwistScore. MAScore represents the mean score of individual β-arch scores, which are modified scores generated using the ArchCandy program. Meanwhile, CompactScore1 and CompactScore2 provide two distinct measures to assess the compactness of β-serpentines from different perspectives. Additionally, TwistScore evaluates the impact of fibril twist on the probability of β-serpentine formation.

of forming amyloid structures (Figure S6, Supporting Information). CryoEM studies of Aβ42 fibrils have shown that motifs I and II interact through hydrophobic interactions, forming the fibril core (Figure 6b).[55] In IAPP fibrils, motif II is packed with another motif II in the core structure of the fibrils (Figure 6c).[56] The structures of different spidroins were predicted by Alphafold,[34] which was based on deep learning and initially designed for soluble protein structure prediction. However, the program—BetaSerpentine—predicts potential β-serpentine arrangements of adjacent β-arches assessed by the ArchCandy programe,[57] and has demonstrated its accuracy in predicting the amyloid structure arrangement of various proteins, including Aβ42 and α-synuclein, with a remarkable agreement with corresponding NMR data.[58] Initially, in its soluble state, the MiSp spacer domain adopts an α-helical conformation, where motifs 1 and II are positioned at the end of helix 1 and within the loop between helix 4 and 5, respectively (Figure 6d). Upon fibril formation, both motifs 1 and II are able to form β-serpentine arrangements (Figure 6d) as predicted by BetaSerpentine,[58] suggesting these motifs have the potential to play a significant role in the formation of the amyloid-like structures.

The introduction of amyloid motifs KLVFFAE (corresponds to MiSp spacer motif I) from Aβ and FGAILSS (corresponds to MiSp spacer motif II) from IAPP into spider silk glycine-rich segments has been found to increase the level of crystallinity in the fibers. Recombinant fibers generated from a protein polymer (≈378 kDa) containing 128 repeats of the FGAILSS sequence exhibit a tensile strength of 0.98 ± 0.08 GPa.[54] In our study, the globular MiSp spacer domain formed amyloid-like fibrils (Figure 3e–h), significantly enhancing the strength of the fibers. By fusing a protein with a size of 64 kDa, silk-like fibers were spun with an average mechanical strength of ≈352 MPa (Figure 5e,f). Considering the above observations, it is reasonable to attribute this enhancement, at least in part, to the presence of motifs I and II in the spacer domain. Our results suggest that the MiSp spacer domain is a natural amyloidogenic domain used by spiders to enhance silk properties while directing fibrillization pathways to prevent the formation of cytotoxic intermediates.

3. Conclusion

Spidroins exhibit a pattern consisting of central repetitive regions flanked by NT and CT domains. These repetitive regions can be classified into two types: type I spidroins, which mainly contain motifs rich in Gly, Ala, and Pro, sometimes interspersed with spacers, and type II spidroins that comprise larger repetitive subunits. The spacer domain in MiSp is structurally related to the repetitive subunits of type II spidroins, contains amyloid-forming motifs similar to those observed in human pathogenic amyloid peptides, and has the ability to self-assemble into amyloid fibrils through a nucleation-independent pathway. Importantly, the presence of the MiSp spacer domain can facilitate the assembly of recombinant chimeric spidroins into silk fibers, and significantly enhance their mechanical strength.

The significance of high molecular weight in spidroins for achieving robust mechanical properties is apparently well established. However, our study reveals that molecular homogeneity within silk fibers is also likely a crucial factor in determining mechanical strength, which can be accomplished by incorporating amyloid-forming domains. Hybrid polypeptides combining short pathogenic amyloid motifs and spider silk glycine-rich segments from *T. clavipes* MaSp1 can indeed assemble into β-sheet nanofibrils under constant agitation and be wet-spun into macroscopic fibers with excellent tensile strength.[54,59] Additionally, modifying the amino acid sequence of poly-Ala motif in MaSp1 to enhance its amyloidogenic propensity has shown promise in improving the mechanical properties of biomimetic spider silk fibers.[48] However, it is important to note that amyloid nanofibrils are inherently toxic and possess self-seeding and cross-seeding capabilities, potentially associated with various amyloid diseases. In our previous investigations, the amyloid-like nanofibrils formed by spidroins were not able to self- or cross-seed fibril formation and did not significantly exhibit toxicity compared to those derived from amyloidogenic peptides linked to human diseases.[36] The primary distinctions between these two types of nanofibrils lie in their amino acid sequences and the mechanisms underlying fibril formation. Spidroins follow a non-nucleation-dependent isodesmic aggregation pathway, while amyloidogenic peptides associated with diseases employ a nucleation-dependent amyloid formation pathway. Notably, both types can assemble into solid macroscopic silk-like fibers composed of nanofibrils. However, the in vivo responses to these fibers, particularly regarding cross-seeding effects, may differ. Since silk nanofibrils derived from cocoons have been found to accelerate amyloid formation in vivo,[60] it is crucial to consider the possibility of cross-seeding effects, particularly for fibers derived from pathogenic amyloid peptides. The MiSp spacer domain found in *A. ventricosus* represents a natural biocompatible globular amyloidogenic domain likely utilized by spiders to enhance mechanical strength and holds great promise for the fortification of a wide range of functional materials.

4. Experimental Section

AlphaFold Modeling and Sequence Analysis: The structures of terminal domains, repetitive regions, and the spacer regions of different spidroins from *A. ventricosus* were predicted using AlphaFold2[34] (https://github.com/sokrypton/ColabFold[61]), and visualized and analyzed by ChimeraX.[62] The sequence alignments (Muscle methods) and phylogenetic RAxML analysis were performed by Geneious Prim 2023.1.2. Amyloidogenic regions of the MiSp spacer domain were predicted by a consensus method AMYLPRED2 that employs a consensus of different methods specifically developed to predict features related to the formation of amyloid fibrils (http://thalis.biol.uoa.gr/AMYLPRED2/).[63] The spacer domain's amyloidogenic structure was predicted using BetaSerpentine, a tool that forecasts potential β-serpentine arrangements of adjacent β-arches.[58] The default values for the individual β-arches and β-serpentines thresholds were set to 0.0 and 0.2, respectively.

Protein Sequence and Construct Preparation: The non-repetitive NT (N) domain, the repetitive region (M) covering typical MiSp motifs, a spacer domain (S) located in the middle of the repetitive region, and the non-repetitive CT (C) domain of *A. ventricosus* MiSp (GenBank access No. JX513956) were customized, and the relevant amino acid sequences are given in Table S1 (Supporting Information). Gene fragments encoding Trx-spacer, NMC, and NMSC were synthesized by Jinweizhi Company (Suzhou, China) and ligated into PET-32a vector through NdeI and XhoI, respectively. The final sequences of the constructs were confirmed by sequencing.

Expression and Purification: The *E. coli* cells expressing Trx-spacer, NMC, or NMSC were inoculated, respectively, into 5 mL LB medium (containing 100 mg L^{-1} ampicillin) and incubated at 37 °C with shaking overnight. The overnight culture was then transferred into fresh 500 mL LB medium with 100 mg L^{-1} ampicillin at a ratio of 1:100. Protein expression was induced with 1 mmol L^{-1} (final concentration) Isopropyl β-D-1-thiogalactopyranoside (IPTG) when OD600 was 0.8–1.0 at 25 °C. The cells were collected by centrifugation (5000 rpm, 20 min) and resuspended in 30 mL 20 mmol L^{-1} Tris pH 8.0.

For recombinant spacer protein preparation, cell suspension was sonicated (65% max power, 2 s on and 2 s off, 12 min) and centrifuged (24 000 g, 30 min, 4 °C) in 20 mmol L^{-1} Tris pH 8.0 twice to wash the pellets. The pellets were resuspended in 20 mmol L^{-1} Tris pH 8.0 with 4 mol L^{-1} urea, sonicated, and centrifuged, and the supernatant was collected which was followed by IMAC purification. After binding to the Ni-NTA column, the Trx-spacer protein was sequentially washed by 20 mmol L^{-1} Tris pH 8.0 containing 2, 1, and 0 mol L^{-1} urea. Then the Ni-NTA column was washed with 20 mmol L^{-1} Tris pH 8.0 containing 20 mmol L^{-1} imidazole, and the target proteins were eluted using 20 mmol L^{-1} Tris pH 8.0 with 300 mmol L^{-1} imidazole. The Trx-spacer was dialyzed against 20 mmol L^{-1} Tris pH 8.0 with 300 mmol L^{-1} NaCl, and cleaved by thrombin (GE Healthcare, 1:600, thrombin: protein, w/w) overnight at 4 °C. The final tag-free spacer was purified by a second Ni-NTA column (reverse-IMAC), where the spacer proteins were present in the flowthrough. Finally, the tag-free spacer proteins were isolated by SEC (superdex75 column (26/600)) with 20 mmol L^{-1} Tris HCl pH 8.0 as running buffer.

For NMC and NMSC, due to the formation of inclusion bodies, after sonication and centrifugation, the pellets were collected. The inclusion bodies were washed by 10 mmol L^{-1} Tris pH 8.0, 1% Triton X-100, 100 mmol L^{-1} NaCl, 1 mmol L^{-1} EDTA, and 1 mol L^{-1} urea three times. Then the inclusion bodies were resuspended in 10 mmol L^{-1} Tris with 8 mol L^{-1} urea at pH 8.0, and centrifuged (12 000 rpm, 10 min, 4 °C), after which the target proteins were distributed in the supernatant fraction. Gradient dialysis with decreased urea concentrations (4 and 2 mol L^{-1}) was performed, followed by dialysis with water to remove any remaining salt. The dialyzed solution was lyophilized with a freeze-drying instrument (FreeZone 2.5 L Benchtop Freeze Dry System).

Circular Dichroism Spectroscopy: At room temperature (25 °C), circular dichroism (CD) spectra of recombinant MiSp spacer, recombinant NMC, and NMSC from 260 to 190 nm were recorded using a circular dichroism spectrometer (Applied Jasco Ltd, Japan) in a 1 mm cuvette with a wavelength gradient rate of 0.5 nm, response time of 1 s, and bandwidth of 1 nm. The data shown were the average from three scans. Blank was measured under the same conditions and subtracted. To study the secondary structure changes of the recombinant spacer proteins with different incubation time (from 0 to 3000 s) at 37 °C and various temperatures (from 20 to 100 °C, and 20 °C), CD spectra of recombinant spacer were recorded

from 260 to 190 nm in 1 mm path length quartz cuvettes using an Aviv 410 Spectrometer (Lakewood, NJ, USA). The wavelength step was 0.5 nm, averaging time 0.3 s, time constant 100 ms, and bandwidth 1 nm.

ThT Fluorescence Assay and Kinetics Modeling: To evaluate the fibrillar aggregation of the recombinant spacer, the recombinant proteins (1.0–8.0 µmol L^{-1}) in 20 mmol L^{-1} NaPi pH 8.0 with 0.2 mmol L^{-1} EDTA in the presence of 10 µmol L^{-1} ThT were added to each well (20 µL each) of half-area 384-well black polystyrene microplates with clear bottom and non-binding surface (Corning Glass 3766, USA), and incubated at 37 °C under quiescent conditions. The ThT fluorescence was continuously recorded using a 440 nm excitation filter and a 480 nm emission filter (FLUOStar Galaxy from BMG Labtech, Germany). For aggregation mechanism analysis, the traces were fitted by the two-term model – polymerization and conformational change (Equation (1))[36]:

$$F/F_{\infty} = C_0\, e^{-k_r I_0 t} + (1 - C_0)\, e^{-k_c I_0 t} \quad (1)$$

where F and F_{∞} are fluorescence intensity and fluorescence intensity at 200 h extrapolated from the double exponential decay fitting, C_0 – monomer concentration available for polymerization, I_0 – monomer concentration serving as an initiator that was set as a fraction of monomers fitted from previous study (I_0≈12% of starting monomer concentration) of recombinant MiSp repetitive region,[36] k_r – polymerization rate and k_c – conformational change rate. ThT plateau level of kinetic traces was determined using double exponential (Equation (2)) fit of raw data.

$$f\ (t) = Ae^{-b\ t} + Ce^{-d\ t} \quad (2)$$

After fitting intensity of each raw curve was divided by the corresponding value of f(t = 200 h). The data scaled in this way was fitted by model Equation (1).

Electrospray Ionization Mass Spectrometry (ESI-MS): The buffer of 40 µmol L^{-1} spacer protein was exchanged to 200 mmol L^{-1} ammonium acetate adjusted to pH 8.0, 7.0, or 5.5 using Micro Bio-Spin 6 columns (Bio-Rad). Samples were analyzed directly after exchanging the buffer and after incubation for 24 h at 37 °C. Mass spectra were recorded on a Micromass LCT ToF modified for analysis of intact protein complexes (MS Vision, Netherland) equipped with an offline nanospray source. Electrospray ionization capillaries were purchased from Thermo Scientific. The capillary voltage was set to 1.5 kV, the cone voltage to 100 V, and the RF lens to 1.5 kV. The pressure in the ion source was kept at 10.0 mbar. Spectra were visualized using MassLynx 4.1 (Waters, UK).

Transmission Electron Microscope and Scanning Electron Microscopy: After incubation, the recombinant spacer domain samples were applied to carbon-coated copper grids (400 mesh, Analytical Standards) and allowed to incubate for 2 min. The excess solution was removed by blotting with Whatman filter paper (grade 1), followed by two washes with Milli-Q water. For staining, 7 µL of 2% uranyl acetate was added to each grid and left for 45 s before final blotting and air-drying. The grids were then analyzed using a TEM (Jeol JEM2100F at 200 kV). The diameter of the nanofibrils was analyzed using Fiji software.[64] In the case of SEM, the silk-like fibers were air-dried on a silicon slice and sputtered with gold/palladium. The fibers were examined using a Hitachi S-4700 field emission scanning electron microscope (Hitachi, Japan) with an accelerating voltage of 15 kV.

Self-Assembly of NMC and NMSC: The recombinant proteins, NMC, and NMSC, were fully solubilized followed by dialysis against 10 mmol L^{-1} Tris-HCl pH 8.0. Different concentrations of proteins (10 µL each), that is, 0.5, 2.5, 3.5, 10, 15, and 20 mg mL^{-1}, were placed on a glass slide at room temperature. Fiber pulling was attempted from the protein droplets every 10 min using a 10 µL pipette tip until the droplets were completely dry. The resulting recombinant fibers were then observed and imaged using a fluorescent microscope (Nikon Instruments Shanghai Co., Ltd., ECLIPSE Ti series).

For the pH-dependent self-assembly in Eppendorf tubes, 100 µL 5 mg $mL^{-1}$of recombinant NMC or 2.5 mg mL^{-1}NMSC proteins were prepared in phosphate buffer at pH 5.0, 6.0, and 7.0 and incubated for 30 min. The fibers were imaged using an inverted fluorescence microscope (Nikon Instruments Shanghai Co., Ltd., ECLIPSE Ti series) and scanning electron microscopy.

Silk Fiber Preparation and Mechanical Property Test: The lyophilized recombinant NMC or NMSC proteins were dissolved in 100% hexafluoroisopropanol (HFIP) to create protein stocks at different concentrations: 100, 80, 50, and 30 mg mL^{-1}. These solutions were then incubated at 37 °C for several hours and subsequently centrifuged to remove any incompletely dissolved powder. The resulting supernatant containing NMC or NMSC was collected as the wet spinning stock. To optimize the spinning process, the NMC or NMSC proteins at different concentrations were spun into a coagulation bath containing various concentrations of methanol: 100%, 90%, 85%, 80%, and 75%.

For the fibril mechanical property test, the lyophilized protein powder of recombinant NMC or NMSC was dissolved in 100% HFIP to reach to a concentration of 8% w/v (80 mg mL^{-1}), and incubated at 37 °C for 3 h. The protein solution for each was centrifuged (12 000 rpm, 10 min), and the supernatant was collected as wet spinning stock. SDS-PAGE was applied to confirm the presence of proteins and the sign of protein degradation. The spinning stock for each was collected in a 29G syringe with a needle and pushed into the coagulation bath through a uniform pump (Suzhou Xunfei Technology Co., Ltd. XFP01-BD). The spinning rate was 10 µL min^{-1} and the coagulation bath was 85% methanol (v/v). The schematic representation of the spinning device is shown in Figure 5a. The silk collector was set up at a distance (≈12 cm) from the position where the silk-like fibers appeared. The fibers were guided with tweezers throughout the process. The collected fibers were placed at room temperature for ≈30 min.

Before preparing silk-like fiber samples (adhered to specific paper frames) for mechanical property test, fibers were assessed under an optical microscope to screen structurally intact fibers. A laser confocal microscope and Image J[64] were used to estimate the fiber diameters with assuming a circular section. The mechanical properties of the recombinant fibers were tested on the INSTRON-3365 (dual-arm material testing machine), where the temperature was set as 20 ± 2 °C and the humidity was 65 ± 5%. At least 10 samples for each type of recombinant silk-like fibers were tested at a constant strain rate of 10 mm min^{-1}, with the gauge length of 20 mm.

Fourier Transform Infrared Spectroscopy: To evaluate secondary structure composition, the recombinant NMC, and NMSC silk-like fibers were measured by Fourier transform infrared spectroscopy using the VERTEX 70+HYPERION 2000 instrument. Double-sided adhesive was used to adhere fibers to the sample holder and then place them on the ATR attachment for testing. The testing parameters had a scanning frequency of 16 times. Amide I region was used to assign secondary structure elements, where the elements were quantified by the deconvolution results of the absorbance spectra ranging from 1600 to 1700 cm^{-1}. A baseline was subtracted from the spectra and a set of Gaussian peaks was fitted to the absorption curve. Data analysis was performed using the PeakFit routine of the Origin software (Ver. 8.5, OriginLab Corp). Distinct secondary structures exhibited characteristic peaks in the amide I region: 1605–1639 cm^{-1}, 1690–1695 cm^{-1} for β-sheet, 1640–1649 cm^{-1} for random coil, 1650–1658 cm^{-1} for α-helix, and 1659–1689 cm^{-1} for β-turn.[23]

Statistical Analysis: Statistical analyses were performed in Prism 9. Different groups were statistically compared with student t-test. The significance level was set at $p < 0.05$.

Supporting Information

Supporting Information is available from the Wiley Online Library or from the author.

Acknowledgements

This study was supported by the National Nature Science Foundation of China (no. 31771003) and the Priority Academic Program Development of Jiangsu Higher Education Institutions (PAPD). K.W. was supported by the National Natural Science Foundation of China (no. 82371779). G.C.

was supported by the Alzheimer's Association Research Grant, Olle Engkvists Stiftelse, the Petrus and Augusta Hedlunds Stiftelse, Åke Wibergs stiftelse, the Swedish Alzheimer Foundation, the Åhlén Stiftelsens, Karolinska Institutet Research Foundation Grant, the Stiftelsen för Gamla Tjänarinnor, the Stiftelsen Sigurd och Elsa Goljes Minne, the Loo and Hans Osterman Foundation, Geriatric Diseases Foundation at Karolinska Institutet, the Gun and Bertil Stohne's Foundation and the Magnus Bergvall Foundation. X.Z. was supported by the China Scholarship Council. Y.W. was supported by the China Association for Science and Technology.

Conflict of Interest

The authors declare no conflict of interest.

Author Contributions

X.Q., H.W., and K.W. contributed equally to this work. X.Q., H.W., Y.W., A.L., X.Z., R.L., and G.C. performed experiments. X.Q., Y.W., K.W., A.L., I.I., Y.Z., A.R., M.L., J.J., and G.C. analyzed data. X.Q. and G.C. conceived and supervised this study. G.C. wrote the manuscript. All authors commented on the manuscript.

Data Availability Statement

The data that support the findings of this study are available from the corresponding author upon reasonable request.

Keywords

amyloid-like fibril, mechanical property, recombinant spider silk, spacer, spidroin

Received: December 4, 2023
Revised: January 28, 2024
Published online: February 20, 2024

[1] T. Lefèvre, M. Auger, *Int. Mater. Rev.* **2016**, *61*, 127.
[2] M. Andersson, G. Chen, M. Otikovs, M. Landreh, K. Nordling, N. Kronqvist, P. Westermark, H. Jornvall, S. Knight, Y. Ridderstrale, L. Holm, Q. Meng, K. Jaudzems, M. Chesler, J. Johansson, A. Rising, *PLoS Biol.* **2014**, *12*, e1001921.
[3] F. Vollrath, D. P. Knight, *Nature* **2001**, *410*, 541.
[4] O. Tokareva, M. Jacobsen, M. Buehler, J. Wong, D. L. Kaplan, *Acta Biomater.* **2014**, *10*, 1612.
[5] A. Rising, J. Johansson, *Nat. Chem. Biol.* **2015**, *11*, 309.
[6] G. V. Guinea, M. Elices, G. R. Plaza, G. B. Perea, R. Daza, C. Riekel, F. Agullo-Rueda, C. Hayashi, Y. Zhao, J. Perez-Rigueiro, *Biomacromolecules* **2012**, *13*, 2087.
[7] M. Ramezaniaghdam, N. D. Nahdi, R. Reski, *Front. Bioeng. Biotechnol.* **2022**, *10*, 835637.
[8] A. P. Kiseleva, P. V. Krivoshapkin, E. F. Krivoshapkina, *Front. Chem.* **2020**, *8*, 554.
[9] T. Arndt, K. Jaudzems, O. Shilkova, J. Francis, M. Johansson, P. R. Laity, C. Sahin, U. Chatterjee, N. Kronqvist, E. Barajas-Ledesma, R. Kumar, G. Chen, R. Stromberg, A. Abelein, M. Langton, M. Landreh, A. Barth, C. Holland, J. Johansson, A. Rising, *Nat. Commun.* **2022**, *13*, 4695.
[10] T. Arndt, U. Chatterjee, O. Shilkova, J. Francis, J. Lundkvist, D. Johansson, B. Schmuck, G. Greco, Å. E. Nordberg, Y. Li, L. U. Wahlberg, M. Langton, J. Johansson, C. Götherström, A. Rising, *Adv. Funct. Mater.* **2023**, 2303622.
[11] J. L. Yarger, B. R. Cherry, A. van der Vaart, *Nat. Rev. Mater.* **2018**, *3*, 18008.
[12] T. B. Aigner, E. DeSimone, T. Scheibel, *Adv. Mater.* **2018**, *30*, 1704636.
[13] L. Eisoldt, A. Smith, T. Scheibel, *Mater. Today* **2011**, *14*, 80.
[14] B. Schmuck, G. Greco, A. Barth, N. M. Pugno, J. Johansson, A. Rising, *Mater. Today* **2021**, *50*, 16.
[15] M. Andersson, Q. Jia, A. Abella, X. Y. Lee, M. Landreh, P. Purhonen, H. Hebert, M. Tenje, C. V. Robinson, Q. Meng, G. R. Plaza, J. Johansson, A. Rising, *Nat. Chem. Biol.* **2017**, *13*, 262.
[16] A. Heidebrecht, L. Eisoldt, J. Diehl, A. Schmidt, M. Geffers, G. Lang, T. Scheibel, *Adv. Mater.* **2015**, *27*, 2189.
[17] X. Li, X. Qi, Y. M. Cai, Y. Sun, R. Wen, R. Zhang, J. Johansson, Q. Meng, G. Chen, *ACS Biomater. Sci. Eng.* **2022**, *8*, 119.
[18] C. Zhang, J. Mi, H. Qi, J. Huang, S. Liu, L. Zhang, D. Fan, *Int. J. Biol. Macromol.* **2020**, *154*, 698.
[19] W. Finnigan, A. D. Roberts, C. Ligorio, N. S. Scrutton, R. Breitling, J. J. Blaker, E. Takano, *Sci. Rep.* **2020**, *10*, 10671.
[20] Y. Z. Zhou, A. Rising, J. Johansson, Q. Meng, *Biomacromolecules* **2018**, *19*, 2825.
[21] S. Xu, X. Li, Y. Zhou, Y. Lin, Q. Meng, *Biochimie* **2020**, *168*, 251.
[22] X. X. Xia, Z. G. Qian, C. S. Ki, Y. H. Park, D. L. Kaplan, S. Y. Lee, *Proc. Natl. Acad. Sci. U. S. A.* **2010**, *107*, 14059.
[23] Y. Zhou, A. Rising, J. Johansson, Q. Meng, *Biomacromolecules* **2018**, *19*, 2825.
[24] P. L. Babb, N. F. Lahens, S. M. Correa-Garhwal, D. N. Nicholson, E. J. Kim, J. B. Hogenesch, M. Kuntner, L. Higgins, C. Y. Hayashi, I. Agnarsson, B. F. Voight, *Nat. Genet.* **2017**, *49*, 895.
[25] N. A. Ayoub, J. E. Garb, R. M. Tinghitella, M. A. Collin, C. Y. Hayashi, *PLoS One* **2007**, *2*, e514.
[26] G. Chen, X. Liu, Y. Zhang, S. Lin, Z. Yang, J. Johansson, A. Rising, Q. Meng, *PLoS One* **2012**, *7*, e52293.
[27] C. Y. Hayashi, R. V. Lewis, *BioEssays* **2001**, *23*, 750.
[28] C. Y. Hayashi, R. V. Lewis, *Science* **2000**, *287*, 1477.
[29] K. Wang, R. Wen, Q. Jia, X. Liu, J. Xiao, Q. Meng, *Genes* **2019**, *10*, 425.
[30] R. Wen, K. Wang, Q. Meng, *Int. J. Biol. Macromol.* **2020**, *160*, 806.
[31] R. Wen, K. Wang, Q. Meng, *Int. J. Biol. Macromol.* **2020**, *157*, 60.
[32] T. Lefèvre, M. Pézolet, *Soft Matter* **2012**, *8*, 6350.
[33] C. Y. Hayashi, N. H. Shipley, R. V. Lewis, *Int. J. Biol. Macromol.* **1999**, *24*, 271.
[34] J. Jumper, R. Evans, A. Pritzel, T. Green, M. Figurnov, O. Ronneberger, K. Tunyasuvunakool, R. Bates, A. Zidek, A. Potapenko, A. Bridgland, C. Meyer, S. A. A. Kohl, A. J. Ballard, A. Cowie, B. Romera-Paredes, S. Nikolov, R. Jain, J. Adler, T. Back, S. Petersen, D. Reiman, E. Clancy, M. Zielinski, M. Steinegger, M. Pacholska, T. Berghammer, S. Bodenstein, D. Silver, O. Vinyals, et al., *Nature* **2021**, *596*, 583.
[35] M. Baek, F. DiMaio, I. Anishchenko, J. Dauparas, S. Ovchinnikov, G. R. Lee, J. Wang, Q. Cong, L. N. Kinch, R. D. Schaeffer, C. Millan, H. Park, C. Adams, C. R. Glassman, A. DeGiovanni, J. H. Pereira, A. V. Rodrigues, A. A. van Dijk, A. C. Ebrecht, D. J. Opperman, T. Sagmeister, C. Buhlheller, T. Pavkov-Keller, M. K. Rathinaswamy, U. Dalwadi, C. K. Yip, J. E. Burke, K. C. Garcia, N. V. Grishin, P. D. Adams, et al., *Science* **2021**, *373*, 871.
[36] X. Qi, Y. Wang, H. Yu, R. Liu, A. Leppert, Z. Zheng, X. Zhong, Z. Jin, H. Wang, X. Li, X. Wang, M. Landreh, L. A. Morozova-Roche, J. Johansson, S. Xiong, I. Iashchishyn, G. Chen, *Small* **2023**, *19*, e2304031.
[37] M. Otikovs, G. Chen, K. Nordling, M. Landreh, Q. Meng, H. Jörnvall, N. Kronqvist, A. Rising, J. Johansson, K. Jaudzems, *ChemBioChem* **2015**, *16*, 1720.
[38] X. Li, J. S. Fan, M. Shi, C. C. Lai, J. Li, Q. Meng, D. Yang, *Biomacromolecules* **2022**, *23*, 1643.

[39] Y. Yang, Z. Gao, D. Yang, *Int. J. Biol. Macromol.* **2023**, *242*, 124775.
[40] S. Wang, W. Huang, D. Yang, *J. Biomol. NMR* **2012**, *54*, 415.
[41] Z. Lin, W. Huang, J. Zhang, J. S. Fan, D. Yang, *Proc. Natl. Acad. Sci. U. S. A.* **2009**, *106*, 8906.
[42] A. D. Roberts, W. Finnigan, P. P. Kelly, M. Faulkner, R. Breitling, E. Takano, N. S. Scrutton, J. J. Blaker, S. Hay, *Mater. Today Bio* **2020**, *7*, 100068.
[43] M. L. Tremblay, L. Xu, T. Lefevre, M. Sarker, K. E. Orrell, J. Leclerc, Q. Meng, M. Pezolet, M. Auger, X. Q. Liu, J. K. Rainey, *Sci. Rep.* **2015**, *5*, 11502.
[44] C. Y. Hayashi, *Exs* **2002**, *92*, 209.
[45] C. Frieden, *Protein Sci.* **2007**, *16*, 2334.
[46] S. I. Cohen, S. Linse, L. M. Luheshi, E. Hellstrand, D. A. White, L. Rajah, D. E. Otzen, M. Vendruscolo, C. M. Dobson, T. P. Knowles, *Proc. Natl. Acad. Sci. U. S. A.* **2013**, *110*, 9758.
[47] S. I. Cohen, M. Vendruscolo, M. E. Welland, C. M. Dobson, E. M. Terentjev, T. P. Knowles, *J. Chem. Phys.* **2011**, *135*, 065105.
[48] T. Arndt, G. Greco, B. Schmuck, J. Bunz, O. Shilkova, J. Francis, N. M. Pugno, K. Jaudzems, A. Barth, J. Johansson, A. Rising, *Adv. Funct. Mater.* **2022**, *32*, 2200986.
[49] B. Schmuck, G. Greco, T. B. Pessatti, S. Sonavane, V. Langwallner, T. Arndt, A. Rising, *Adv. Funct. Mater.* **2023**, 2305040.
[50] V. Hauptmann, N. Weichert, M. Menzel, D. Knoch, N. Paege, J. Scheller, U. Spohn, U. Conrad, M. Gils, *Transgenic Res.* **2013**, *22*, 369.
[51] C. H. Bowen, T. J. Reed, C. J. Sargent, B. Mpamo, J. M. Galazka, F. Zhang, *ACS Synth. Biol.* **2019**, *8*, 2651.
[52] S. Lin, G. Chen, X. Liu, Q. Meng, *Biopolymers* **2016**, *105*, 385.
[53] X. Zhang, L. Xia, B. A. Day, T. I. Harris, P. Oliveira, C. Knittel, A. L. Licon, C. Gong, G. Dion, R. V. Lewis, J. A. Jones, *Biomacromolecules* **2019**, *20*, 2252.
[54] J. Li, Y. Zhu, H. Yu, B. Dai, Y. S. Jun, F. Zhang, *ACS Nano* **2021**, *15*, 11843.
[55] L. Gremer, D. Schölzel, C. Schenk, E. Reinartz, J. Labahn, R. B. G. Ravelli, M. Tusche, C. Lopez-Iglesias, W. Hoyer, H. Heise, D. Willbold, G. F. Schröder, *Science* **2017**, *358*, 116.
[56] Q. Cao, D. R. Boyer, M. R. Sawaya, R. Abskharon, L. Saelices, B. A. Nguyen, J. Lu, K. A. Murray, F. Kandeel, D. S. Eisenberg, *Nat. Struct. Mol. Biol.* **2021**, *28*, 724.
[57] A. B. Ahmed, N. Znassi, M. T. Chateau, A. V. Kajava, *Alzheimer's Dementia* **2015**, *11*, 681.
[58] S. A. Bondarev, O. V. Bondareva, G. A. Zhouravleva, A. V. Kajava, *Bioinformatics* **2018**, *34*, 599.
[59] B. Dai, C. J. Sargent, X. Gui, C. Liu, F. Zhang, *Biomacromolecules* **2019**, *20*, 2015.
[60] K. Lundmark, G. T. Westermark, A. Olsen, P. Westermark, *Proc. Natl. Acad. Sci. U. S. A.* **2005**, *102*, 6098.
[61] M. Mirdita, K. Schütze, Y. Moriwaki, L. Heo, S. Ovchinnikov, M. Steinegger, *Nat. Methods* **2022**, *19*, 679.
[62] E. F. Pettersen, T. D. Goddard, C. C. Huang, E. C. Meng, G. S. Couch, T. I. Croll, J. H. Morris, T. E. Ferrin, *Protein Sci.* **2021**, *30*, 70.
[63] A. C. Tsolis, N. C. Papandreou, V. A. Iconomidou, S. J. Hamodrakas, *PLoS One* **2013**, *8*, e54175.
[64] J. Schindelin, I. Arganda-Carreras, E. Frise, V. Kaynig, M. Longair, T. Pietzsch, S. Preibisch, C. Rueden, S. Saalfeld, B. Schmid, J. Y. Tinevez, D. J. White, V. Hartenstein, K. Eliceiri, P. Tomancak, A. Cardona, *Nat. Methods* **2012**, *9*, 676.